KU LEUVEN

FACULTY OF SCIENCE
Department of Chemistry

# Computational Exploration of Non-Valence Anions from Biological Quinones

## A Second Order Approximate Coupled Clouster Study



**Mauro Gascón Navas**

Dissertation presented in partial fulfillment
of the requirements for the degree of
Erasmus Mundus Master of Science in
Theoretical Chemistry and Computational
Modelling

Supervisors:
Robin Moorby
Prof. Dr. Thomas Jagau

June 2025

# COMPUTATIONAL EXPLORATION OF NON-VALENCE ANIONS FROM BIOLOGICAL QUINONES

## A SECOND ORDER APPROXIMATE COUPLED CLUSTER STUDY

Mauro GASCON NAVAS

Supervisors:
Robin Moorby
Prof. Dr. Thomas Jagau

Members of the
Examination Committee:
Prof. dr. ir. The Chairman, chair
Prof. dr. ir. The One
Prof. dr. ir. The Other
Prof. dr. External Jurymember
(Far Away)

Dissertation presented in partial fulfillment of the requirements for the degree of Erasmus Mundus Master of Science in Theoretical Chemistry and Computational Modelling

June 2025

Uitgegeven in eigen beheer, Mauro Gascón Navas, Leuven (Belgium)

# Acknowledgements

. . .

Thank you thank you.

**Instructions by the Arenberg Doctoral School:**

The scientific abstract should present the most important aims and conclusions of the dissertation in a brief text of ca. 2 pages.

# Abstract

...

**Instructions by the Arenberg Doctoral School:**

The scientific abstract should present the most important aims and conclusions of the dissertation in a brief text of ca. 2 pages.

# Beknopte samenvatting

. . . aaa

**Instructions by the Arenberg Doctoral School:**

The scientific abstract should present the most important aims and conclusions of the dissertation in a brief text of ca. 2 pages.

# List of Abbreviations

**MD** molecular dynamics. 4

# Contents

**Acknowledgements** i

**Abstract** iii

**Beknopte samenvatting** v

**List of Abbreviations** vii

**Contents** ix

**List of Figures** xi

**List of Tables** xiii

**1 Introduction** 1
- 1.1 Non-Valence Anions . . . 1
  - 1.1.1 Dipole-Bound Anions . . . 2
  - 1.1.2 Approaches to Study Non-Valence Anions . . . 3
- 1.2 Non-Valence Anions in Biology . . . 4
  - 1.2.1 Overlap with Biochemical Systems . . . 4
- 1.3 Biological Quinones . . . 4
  - 1.3.1 Role of Quinones . . . 5
  - 1.3.2 Structural Aspects of Ubiquinone . . . 5

**2 Theoretical Background** 7
- 2.1 Self Consistent Field Methods . . . 7
  - 2.1.1 Electron Correlation . . . 9
  - 2.1.2 Møller-Plesset Perturbation Theory . . . 9
  - 2.1.3 Density Functional Theory . . . 10
  - 2.1.4 Configuration Interaction . . . 10
  - 2.1.5 Coupled Cluster Theory . . . 11

2.1.6 Second Approximate Coupled Cluster . . . . . 13
2.2 Equation-of-Motion Methods . . . . . 13
2.3 Dyson Orbitals . . . . . 14
2.3.1 EOM-CC2 Dyson Orbital Equations . . . . . 15

**3 Computational Methods** **21**

**4 Results and Discussion** **23**
4.1 Performance of EOM-CC2 Related Methods . . . . . 23
4.1.1 Basis Set Dependence of EA-EOM-CC2 in Dipole Bound Anions . . . . . 23
4.1.2 Performance of EA-EOM-CC2 on Valence Bound Radical Anion States of Quinones . . . . . 25
4.1.3 Photoelectron Cross-section Calculations from EOM-CC2/CCSD . . . . . 26
4.2 Study on the Anion States of Ubiquinone . . . . . 26
4.2.1 Energy and Dipole Surfaces of CoQ . . . . . 26
4.2.2 A Simple Cluster Model . . . . . 26
4.2.3 Interaction with Water . . . . . 26
4.2.4 Effect of Nearby Amionacids . . . . . 26

**5 This is conclusion** **31**

**A This is myappendix** **33**

**Bibliography** **35**

# List of Figures

1.1 Classification of non-valence anions . . . . . 2
1.2 Short caption for Table of Figures . . . . . 5
1.3 Short caption for Table of Figures . . . . . 6

2.1 EOM-EA. . . . . 14

4.1 figure valence anion state quinones . . . . . 25
4.2 Surfaces of Q0 . . . . . 27
4.3 Surfaces of Q1 . . . . . 28
4.4 Short caption for Table of Figures . . . . . 29

# List of Tables

2.1 Computational Scaling of Methods . . . . . 12

4.1 EOM-EA DBA basis set dependence. . . . . 24
4.2 table valence anion state quinones . . . . . 25

# Chapter 1

# Introduction

This chapter aims to provide an overview of non-valence anions, with a specific emphasis on dipole-bound anions (DBAs). The relevance of these anions in biological systems is explored, followed by an introduction to the system of interest, namely biological quinones, and their critical role in biological processes. Finally, the research objectives are outlined.

## 1.1 Non-Valence Anions

An anion is an atom or a molecule containing one or more excess electrons. The binding of an excess electron to a neutral molecule can be understood as a competition between the attractive potential of the excess electron to the nuclei and the repulsive forces from the neutral molecule's electrons. Unlike valence electrons in neutral species, these "extra" electrons do not experience a -1/r Coulombic attraction at large distances and instead interact through weaker charge-multipole potentials, which are weaker than the covalent bonds that hold the molecule together [1, 2]. The binding energy of the excess electron is often significantly lower than the ionization energy of the neutral molecule. This makes the molecule undergo changes, ranging from a geometry relaxation, to chemical reaction with the surrounding species. In discussing molecular anions, the concept of electron affinity (EA) is fundamental. On one hand, the adiabatic electron affinity (AEA) quantifies the energy difference between the parent molecule and its corresponding anion, with both species in their electronic ground states and lowest rovibrational levels. On the other hand, the vertical electron affinity (VEA), is defined at the neutral equilibrium geometry,

and is specially relevant for the dynamics of the electron capturing process. A molecule possessing a positive EA is considered electronically stable, as it necessitates an input of energy to remove an electron from the anionic state [1].

Molecular anions can be classified into two distinct categories: valence anions, where the excess electron occupies a compact orbital similar to the other valence molecular orbitals, and non-valence anions (NVA) , where the excess electron occupies a diffuse orbital spatially separated from the molecule. Non-valence anions are further categorized based on the predominant long-range interaction responsible for electron binding: dipole-bound states (DBS), quadrupole-bound states (QBS), and correlation-bound states (CBS). Note that they do not have a rigurous definition, and a NVA is usually stabilized by range of interactions [1, 2, 3, 4, 5].

**Fig w diferent NVAs orbitals goes here**

Figure 1.1: Classification of non-valence anions.

### 1.1.1 Dipole-Bound Anions

From the types of non-valence anions, dipole-bound anions (DBAs) are the most common and well-studied. The initial theoretical framework for non-valence bound states was proposed in 1947 by Fermi and Teller, who demonstrated that a dipole could bind an excess electron if the dipole moment surpasses 1.625 D [6]. Further investigations refined the concept applying to "real" molecules, leading to a critical dipole moment of around 2.5 D[5].

Their "weak" forces that support the binding of the excess electron are responsible for the diffusive nature of the associated orbitals, often extending several Å from the neutral molecule, as well as their relative low energy, usually lower than 0.1 eV. This characteristic renders them particularly susceptible to external perturbations, such as solvent interactions or external electric fields, which can significantly influence their stability and reactivity [1, 2, 5].

Given that DBAs are bound with an energy in the range of the ambient energy ($k_bT \sim 23\,meV$), they may appear to be a theoretical curiosity with limited prectical relavance, whose fate is to undergo a rapid autodetachment. However, there are other possible and interesting paths for some systems, such as a nonadiabatic transition to a stable valence anion state[2, 5]. In this sense, the DBSs act as "Doorway" states for electron capture and transfer processes[5, 7].

This behaviour has made DBA to spawn interest in diverse fields from astrochemistry [8] to radiation biology [9, 10]. When solvent effects are

considered, distinct scenarios emerge. The electron may either (a) localize within the DB orbital, (b) be captured by solvent molecules forming a solvation cage, or (c) interact with solvent molecules whose instantaneous dipole orientations stabilize the DB state. The latter two phenomena are linked to charge-transfer-to-solvent (CTTS) electronic transitions [11, 12].

Additionally, solvated electrons, which may be considered a form of non-valence states, are hypothesized to reside in cavities approximately 2.5 Å in size [13].

### 1.1.2 Approaches to Study Non-Valence Anions

Significant advancements have been achieved in experimental and theoretical methodologies for elucidating the structure and dynamics of NBS. Experimentally, high-resolution photodetachment and photoelectron spectroscopies, in conjunction with cryogenically cooled ion traps and velocity-map imaging, have enabled detailed characterization of NBS rovibrational structures. These techniques have proven instrumental in resolving sharp Feshbach resonances and identifying mode-specific vibrational autodetachment pathways.

The advent of time-resolved pump-probe photoelectron spectroscopy has further advanced the field by capturing ultrafast dynamics of electron detachment and transfer in NBS. Sub-picosecond timescales have been observed for electron transfer from DBS to valence-bound states in nucleobase-containing clusters, highlighting the transient role of NBS in electron-driven processes. Additionally, picosecond-resolved measurements have quantified autodetachment lifetimes in vibrationally specific manners, as demonstrated in phenoxide systems [5, 14]. Recent advances in spectroscopy have facilitated the study of NBS in the gas phase, generating significant interest in their properties [7].

Their ab initio descriptions often require particular attention due to the more diffuse nature of the associated orbitals [1, 4].

The theoretical investigation of DBAs presents two primary challenges. First, atomic orbital basis sets must be sufficiently diffuse to accurately describe the spatial extent of the DB orbital, often necessitating the use of custom basis sets [15]. Although the electron in the DB orbital resides predominantly far from the precursor's valence electrons, it exhibits significant dispersion-like interactions with these electrons, contributing substantially to the electron binding energy (EBE). This interaction reflects the polarizable nature of the DB orbital, which engages in pronounced van der Waals interactions with nearby electron densities [16]. Theoretical investigations have complemented experimental efforts through high-level quantum chemical techniques such as equation-of-motion coupled-cluster (EOM-CC) and density functional theory

(DFT) [17]. Autodetachment processes have been modeled using Fermi's golden rule, with detachment rates linked to nuclear displacements of the electron-binding potential. These approaches have provided predictive frameworks for mode-specific detachment behaviors, particularly in DBS and QBS, where angular dependencies and induced dipole effects play critical roles.

## 1.2 Non-Valence Anions in Biology

Research on DBAs has predominantly focused on gas-phase systems. In biological contexts, DBAs have been studied for their interactions with DNA, particularly in radiation damage and radiosensitization [9, 10].

The survival of NBS in condensed matter remains a subject of debate. Computational studies suggest that hydration influences the localization of the excess electron, often displacing it onto the solvent cage's surface [18]. Conversely, experimental evidence indicates that alkyl chains do not disrupt DBS stability [19], and DBS-mediated mechanisms have been observed in solvated uracil systems [20]. The viability of NBS in bulk systems depends on the molecular density and polarity of the medium. While apolar solvents may hinder DBS existence due to excluded volume effects, polar solvents can stabilize DBS through dipolar interactions, analogous to CTTS states [11, 12].

The role of NBS in natural biological pathways remains largely unexplored. Their sensitivity to environmental factors suggests potential applications in regulating long-range electron transfer processes, particularly in soft matter systems such as proteins, which feature vacant pockets capable of accommodating DBS.

### 1.2.1 Overlap with Biochemical Systems

Studies on electron interactions with biomolecules, both in bare and hydrated states, have highlighted the significance of DBAs in biological systems [21]. For instance, DBAs have been implicated in the electron transfer processes of flavins [22].

## 1.3 Biological Quinones

The term "quinone" originates from quinic acid, first identified in Cinchona bark in 1785 and later analyzed by Liebig [23, 24]. Quinones are ubiquitous in

biological systems and play vital roles as electron carriers in redox reactions [25].

### 1.3.1 Role of Quinones

Quinones facilitate electron and proton transfer between enzymes, serving as key intermediates in biochemical redox processes.

### 1.3.2 Structural Aspects of Ubiquinone

Coenzyme Q (ubiquinone), a prevalent quinone in nature, stabilizes both valence and dipole-bound anionic states due to its unique structure. This renders it an intriguing subject for NBS studies. Experimental observations have confirmed the presence of DBAs in 2-3-dimethoxy-para-benzoquinone (CoQ0), with diminished stability in CoQ1 and CoQ2 [26, 27, 28, 29].

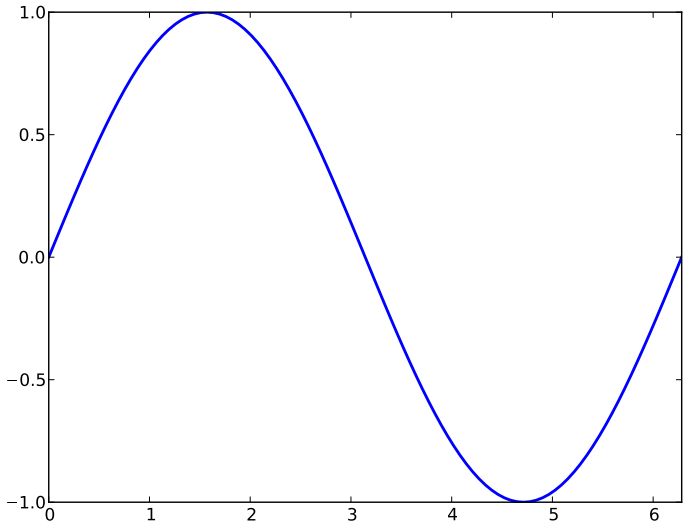


Figure 1.2: Illustration of how to include a figure (long text, should not go to Table of Figures).

Introducing some symbol: $\Theta$.

Introducing an acronym: MD.

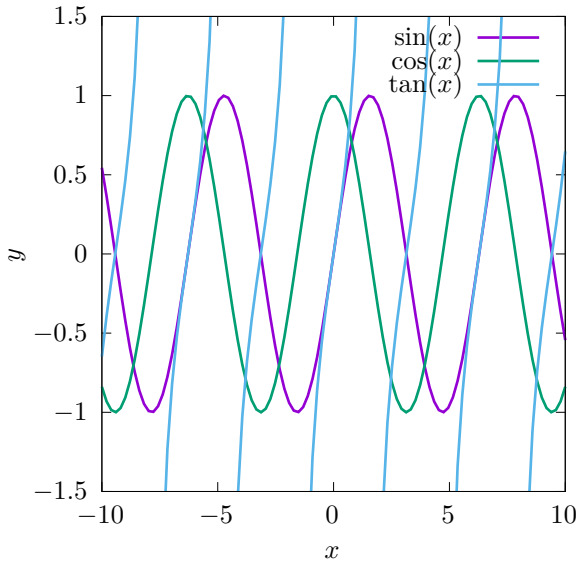


Figure 1.3: Illustration of how to include a figure (long text, should not go to Table of Figures).

# Chapter 2

# Theoretical Background

## 2.1 Self Consistent Field Methods

The objective of any quantum chemical calculation is to solve the time-independent Schrödinger equation (TISE) for a many-electron system:

$$\hat{H}\Psi = E\Psi \tag{2.1}$$

However, solving the TISE exactly for systems with more than one electron is computationally infeasible due to the complexity of electron-electron interactions. To address this, approximate methods such as the Hartree-Fock (HF) method have been developed[30].

The Hartree-Fock (HF) method stands as the cornestone electronic structure calculations. Its primary objective is to provide an approximate solution to the many-electron time-independent Schrödinger equation within the Born-Openhaimer approximation, which governs the behavior of electrons within atoms and molecules: The HF method achieves this by assuming that each electron moves independently within an average electrostatic field generated by the other electrons in the system. In the HF method the $N$-electron wavefunction is represented by a Slater determinant, which is formed by taking the antisymmetrized product of N individual one-electron spin-orbitals ($\chi$):

$$\Psi(\mathbf{r}_1, \mathbf{r}_2, \ldots, \mathbf{r}_N) = \frac{1}{\sqrt{N!}} \begin{vmatrix} \chi_1(\mathbf{r}_1) & \chi_2(\mathbf{r}_1) & \cdots & \chi_N(\mathbf{r}_1) \\ \chi_1(\mathbf{r}_2) & \chi_2(\mathbf{r}_2) & \cdots & \chi_N(\mathbf{r}_2) \\ \vdots & \vdots & \ddots & \vdots \\ \chi_1(\mathbf{r}_N) & \chi_2(\mathbf{r}_N) & \cdots & \chi_N(\mathbf{r}_N) \end{vmatrix} \tag{2.2}$$

The choice of using a deteminant inherently satisfies both the Pauli exclusion principle, and the antisymmetry requirement of fermions. The energy expectation for a Slater determinant according to HF is variational and can be computed as:

$$\begin{aligned} E_{HF} &= \langle\Psi|\sum_{i=1}^{N}\hat{F}_i|\Psi\rangle \\ &= \langle\Psi|\sum_{i=1}^{N}\hat{h}(i) + \sum_{i,j=1}^{N}(2\hat{J}_j(i) - \hat{K}_j(i))|\Psi\rangle \\ &= \sum_{i=1}^{N}\langle\chi_i|\hat{h}|\chi_i\rangle + \frac{1}{2}\sum_{i,j=1}^{N}\langle\chi_i\chi_j||\chi_i\chi_j\rangle \end{aligned} \tag{2.3}$$

Where, $\hat{F}$ is the Fock operator. $\hat{F}$ is made up from $\hat{h}$, the one-electron core Hamiltonian operator (kinetic energy and electron-nucleus attraction); $\hat{J}_j(i)$, the Coulomb operator, describing the electrostatic repulsion between electron i and the average charge distribution of electron j, and $\hat{K}_j(i)$ is the exchange operator, a purely quantum mechanical term arising from the antisymmetry principle. Because of the two electron terms, the computational cost of HF scales as $O(N^4)$.

The Hartree-Fock equations are inherently non-linear: because the Fock operator depends on the wavefunctions of all the other electrons, their interactions are coupled. Consequently, these equations cannot be solved analytically and are solved using an iterative procedure known as the self-consistent field (SCF) method, where the final field experienced by the electrons must be consistent with the electron distribution that generates that field. The SCF procedure involves the following steps: An initial guess for the spin-orbitals is made. Using this initial guess, the Fock operator is constructed. The Hartree-Fock equations are then solved by diagonalizing the Fock operator to obtain a new set of molecular orbitals and their corresponding energies. This new set of orbitals is compared to the previous set. If the change is below a predefined threshold, the procedure is considered converged, and the SCF is achieved. If convergence is not reached, the new set of orbitals is used to construct a new Fock operator, and the process is repeated. Convergence signifies that a stable electronic configuration has been reached within the limitations of the Hartree-Fock approximation.

In practical Hartree-Fock calculations, the spinorbitals are expressed as linear combinations of predefined mathematical functions known as basis functions. The set of these functions is called a basis set. Because a finite basis set cannot exactly represent the spinorbitals, they greatly define the level of accuracy

and computational cost of the calculation. Larger basis sets generally lead to more accurate descriptions of the electronic structure at the cost of increased computational effort.

### 2.1.1 Electron Correlation

The Hartree-Fock (HF) method is inherently limited by its neglect of the instantaneous interactions of electrons. In the HF approximation, each electron is treated as moving independently within a static, average field created by the other electrons. This mean-field approach fails to account for the fact that electrons will instantaneously repel each other, leading to a correlated movements as they try to avoid each other in space.
The primary consequence of neglecting electron correlation in the HF approximation is an overestimation of the electron-electron repulsion energy. While the HF method does account for the exchange interaction exactly as a consequence of the antisymmetry of the Slater determinant (Fermi correlation), it completely neglects the Coulomb, or dynamic, correlation. This omission leads to a higher electronic energy than the exact solution, and an inability to accurately predict certain phenomena, such as London dispersion forces.
The difference between the exact non-relativistic energy of the system and the energy obtained in the HF complete basis limit is defined as the correlation energy and is always negative due to the variational principle. Correlated methods aim to include the effects of the instantaneous interactions between electrons that are neglected in the mean-field approximation of HF theory. In the following sections, several correlated methods relevant to this work are presented.

### 2.1.2 Møller-Plesset Perturbation Theory

Møller-Plesset (MP) perturbation theory offers a way to improve upon the HF energy by the use of Raylei-Schro perturbation theory: the electron correlation is treated as a perturbation to the HF Hamiltonian. The energy and wavefunction are then expanded as a series in terms of the perturbation strength. The first-order energy correction in MP theory is zero, so the first non-trivial correction to the HF energy appears at the second order, giving rise to the MP2 method. The MP2 energy correction for a closed-shell molecule is given by:

$$E_{\mathrm{MP2}} = -\frac{1}{4}\sum_{ij}^{\mathrm{occ}}\sum_{ab}^{\mathrm{virt}}\frac{|\langle ij||ab\rangle|^2}{\epsilon_a + \epsilon_b - \epsilon_i - \epsilon_j} \tag{2.4}$$

Where $i, j$ denote occupied molecular orbitals, $a, b$ denote virtual molecular orbitals, and $\epsilon$ are the corresponding orbital energies from the HF calculation. MP theory can be extended to higher orders (MP3, MP4, etc.) to achieve greater accuracy, although the computational cost increases significantly with each order. The computational cost of MP2 scales as $O(N^5)$.

### 2.1.3 Density Functional Theory

Density Functional Theory (DFT) provides an alternative approach to incorporating electron correlation by parametrizing the energy on the electron density rather than the wavefunction, reducing the degrees of freedom of the system from $3N - 3$ to just 3. In the most commonly used form of DFT, the Kohn-Sham method, the prpblem is formulated terms of orbitals that are not physical, but are chosen to reproduce the electron density of the system. The fundamental principle of DFT is that the ground state energy of a system is a unique functional of its electron density:

$$\left(-\frac{1}{2}\nabla^2 + \hat{V}_{\text{ext}}(\mathbf{r}) + \hat{V}_{\text{H}}(\mathbf{r}) + \hat{V}_{\text{XC}}[\rho(\mathbf{r})]\right)\psi_i(\mathbf{r}) = \epsilon_i\psi_i(\mathbf{r}) \tag{2.5}$$

Where $\hat{V}_{\text{ext}}$ respresents the external potential, $\hat{V}_{\text{H}}(\mathbf{r}) = \int \frac{\rho(\mathbf{r}')}{|\mathbf{r}-\mathbf{r}'|}d\mathbf{r}'$ is the Hartree potential, $\hat{V}_{\text{XC}}$ is the Exchange-Correlation potential and $\rho(\mathbf{r})$ is the electron density. The exchange-correlation functional is the most challenging part of DFT, as it is not known exactly and must be approximated. The accuracy of DFT calculations depends heavily on the choice of exchange-correlation functional. The computational cost of DFT scales as $O(N^4)$.

### 2.1.4 Configuration Interaction

Configuration Interaction (CI) methods improve upon HF by expressing the electronic wavefunction as a linear combination of the HF ground state determinant and excited state determinants:

$$|\Psi_{\text{CI}}\rangle = c_0|\Phi_0\rangle + \sum_{ia} c_{ia}|\Phi_{ia}\rangle + \sum_{ijab} c_{ijab}|\Phi_{ijab}\rangle + \dots \tag{2.6}$$

Where $|\Phi_0\rangle$ is the HF ground state determinant, $|\Phi_{ia}\rangle$ represents a determinant with a hole in spin-orbital $i$ and a particle in the spin-orbital $a$, and c are the CI coefficients. Full CI (FCI), includes all possible excitations within a given one-electron basis set and represents the exact solution to the non-relativistic Schrödinger equation in that basis. However, is computationally prohibitive

for all but the simplest systems. Full Configuration Interaction (FCI) includes all possible excitations within a given one-electron basis set and represents the exact solution to the non-relativistic Schrödinger equation in that basis. However, it is computationally prohibitive for all but the simplest systems.
Truncated CI methods, such as CISD (singles and doubles), are more practical but lack size extensivity —a property ensuring that the energy of a system scales correctly with the number of non-interacting subsystems. A method is size-extensive if, for two infinitely separated molecules $A$ and $B$, the total energy satisfies $E(A+B) = E(A) + E(B)$. Truncated CI methods fail to satisfy this condition because they do not include all necessary higher-order excitations, leading to an underestimation of the total energy as system size grows.
CI are, however, size-consistent, meaning that the energy behaviour remains consistent when interaction between the involved molecular subsystems is nullified (by distance, for instance). While CISD is size-consistent, its lack of size extensivity makes it unsuitable for extensive systems.

### 2.1.5 Coupled Cluster Theory

Similarly to CI, the coupled cluster CC method expands the wavefunction as a linear combination of Slater determinats. However, the CC wavefunction is size-extensive and size-consistent by using an exponential ansatz,

$$|\Psi_{\mathrm{CC}}\rangle = e^{\hat{T}}|\Psi_0\rangle \tag{2.7}$$

where $\hat{T}$ is the cluster operator, which is the central component of CC theory and is defined as a sum of excitation operators,

$$\hat{T} = \hat{T}_1 + \hat{T}_2 + \hat{T}_3 + \cdots + \hat{T}_N \tag{2.8}$$

where $N$ is the total number of electrons in the system. Each term in this sum corresponds to a specific level of excitation and is expressed within the second quantization formalism:

- $\hat{T}_1 = \sum_i^{\mathrm{occ}} \sum_a^{\mathrm{virt}} t_i^a a_a^\dagger a_i$ represents single excitations.
- $\hat{T}_2 = \frac{1}{4} \sum_{i,j}^{\mathrm{occ}} \sum_{a,b}^{\mathrm{virt}} t_{ij}^{ab} a_a^\dagger a_b^\dagger a_j a_i$ represents double, *coupled* excitations.
- Higher-order excitation operators $\hat{T}_3, \hat{T}_4, \ldots$ describe coupled excitation of three, four, and more electrons, respectively.

The coefficients $t_i^a$, $t_{ij}^{ab}$, etc., are cluster amplitudes to determined by projection of the CC Schrödinger equation onto the excited determinant. The exponential

form, expanded as a Taylor series,

$$e^{\hat{T}} = 1 + \hat{T} + \frac{1}{2!}\hat{T}^2 + \dots \tag{2.9}$$

inherently includes terms that represent disconnected clusters, which are ensures for size consistency. The energy is obtained by projecting onto the HF reference determinant:

$$E_{\text{CC}} = \langle \Psi_0 | e^{-\hat{T}} \hat{H} e^{\hat{T}} | \Psi_0 \rangle \tag{2.10}$$

Using the Baker-Campbell-Hausdorff expansion, the exponential operators in Eq. 2.10 can be simplified to a series of commutators which ends at the fourth order. The cluster operator $\hat{T}$ can be truncated at different levels of excitation:

- **CCD** (Coupled Cluster Doubles): This is the simplest approximation in the CC family, where the cluster operator is truncated to include only double excitations: $\hat{T} \approx \hat{T}_2$. There is no CC Singles since the Brilluin's theorem implies that the amplitudes of single excitations alone are null.
- **CCSD** (Coupled Cluster Singles and Doubles): This is one of the most widely used and generally accurate *ab initio* methods, where the cluster operator includes both single and double excitations: $\hat{T} \approx \hat{T}_1 + \hat{T}_2$.
- **CCSDT** (Coupled Cluster Singles, Doubles, and Triples): $\hat{T} \approx \hat{T}_1 + \hat{T}_2 + \hat{T}_3$.
- ...

The hierarchy can be extended to include even higher levels of excitation, with the properties converging to the FCI limit. The computational cost of CC methods increases rapidly with the level of truncation, as shown in Table 2.1.

| Method | Operation count | Memory |
|---|---|---|
| HF | $O(N^4)$ | $O(N^4)$ |
| DFT | $O(N^4)$ | $O(N^4)$ |
| MP2 | $O(N^5)$ | $O(N^4)$ |
| CCD/CCSD | $O(N^6)$ | $O(N^4)$ |
| CCSDT | $O(N^8)$ | $O(N^6)$ |
| CC2 | $O(N^5)$ | $O(N^4)$ |

Table 2.1: Computational scaling of quantum chemistry methods.

### 2.1.6 Second Approximate Coupled Cluster

Second Approximate Coupled Cluster (CC2) belongs to the broader family of CCn approximate coupled cluster methods, where the 'n' in CCn indicates the truncation of the cluster operator within a perturbative hierarchy. These methods aim to reduce the computational cost associated with standard CC truncations while still retaining a reasonable level of accuracy.

In CC2, the equations for the single amplitudes, $t_i^a$, are the same as CC theory (Eq. 2.7) under the constraint that the doubles amplitudes, $t_{ij}^{ab}$, are calculated using the non-iterative expression for MP2 (Eq 2.4). The resulting expression for the CC2 correlation energy is:

$$E_{\mathrm{CC2}} = \frac{1}{4}\sum_{ij}^{\mathrm{occ}}\sum_{ab}^{\mathrm{virt}}\frac{|\langle ij||ab\rangle|^2}{\epsilon_a+\epsilon_b-\epsilon_i-\epsilon_j} + \sum_{i}^{\mathrm{occ}}\sum_{a}^{\mathrm{virt}}\hat{F}_{ai}t_i^a \tag{2.11}$$

The perturbative treatment of the doubles amplitudes in CC2, reduces the computational cost compared to CCSD, Table 2.1. While this approximation can lead to a less accurate description of electron correlation, the inclusion of singles amplitudes allows for an approximate description of orbital relaxation, which often leads to higher quality wavefunction, and hence properties, compared to MP2.

## 2.2 Equation-of-Motion Methods

Equation-of-Motion Coupled Cluster (EOM-CC) methods are an extension of ground-state coupled cluster theory which provide a framework for calculating a variety of excited (EE), ionized (IP) and electron-attached (EA) states. In the EOM-CC, the target electronic state is generated by applying a linear excitation operator $\hat{R}$ to a reference state, which typically is the coupled cluster wavefunction of the ground state. The target state wavefunction can then be expressed as $|\Psi_{\mathrm{EOM}}\rangle = \hat{R}|\Psi_{\mathrm{CC}}\rangle = \hat{R}e^{\hat{T}}|\Phi_{\mathrm{HF}}\rangle$. Figure 2.1, shows some of the determinats of $|\Psi_{\mathrm{EA}}\rangle$, where the target state has one more $\alpha$ electron.

The form of the operator $\hat{R}$ is similar to the cluster operator and chosen to access the desired target state. In the case of EOM-EA, the electron attachment operator $R^{\mathrm{EA}}$ includes terms that describe the creation of one electron to an unoccupied orbital, terms that describe the creation of one electron accompanied by the excitation of another electron from an occupied to an unoccupied orbital,

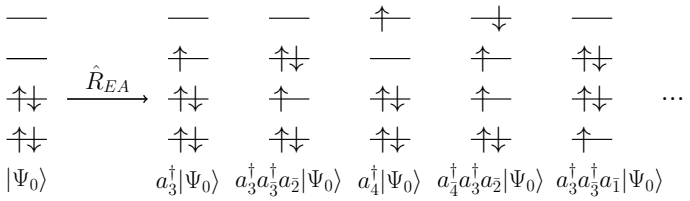


Figure 2.1: EOM-EA.

and so on:

$$\hat{R}^{\mathrm{EA}} = \hat{R}_1^{\mathrm{EA}} + \hat{R}_2^{\mathrm{EA}} + \ldots = \sum_a r^a a_a^\dagger + \frac{1}{2}\sum_{ab}\sum_i r_i^{ba} a_b^\dagger a_a^\dagger a_i + \ldots \tag{2.12}$$

Where $a$ and $b$ denote virtual orbitals, $i$ denotes an occupied orbital, and $r^a$ and $r_i^{ba}$ are the coefficients to be determined. By truncating at the same excitation level as the cluster operator, the method is rigorously size-extensive and size-consistent. The EA energies, or any other EOM energy, can be obtained as the eigenvalues of the similarity-transformed Hamiltonian, $\bar{H}_{\mathrm{N}}$:

$$\bar{H}_{\mathrm{N}}\hat{R}|\Psi_0\rangle = \Delta E_{\mathrm{EOM}}\hat{R}|\Psi_0\rangle \tag{2.13}$$

$$\bar{H}_{\mathrm{N}} = e^{-\hat{T}}\hat{H}e^{\hat{T}} - \langle\Psi_0|e^{-\hat{T}}\hat{H}e^{\hat{T}}|\Psi_0\rangle \tag{2.14}$$

Since the similarity trnasformed hamiltonian is non-hermitian, the left and right are different but correspond to the same eigenvalues. This means that the properties have 'right' and 'left' expectation values.
The strength of the EOM-CC ansatz is the use of a closed shell reference to access open shell states, which are eigenfunctions of the $\hat{S}^2$ operator. The EOM-CC methods are also size-extensive and size-consistent. The computational cost of EOM-CC methods is similar to that of the corresponding ground-state CC methods.

## 2.3 Dyson Orbitals

Dyson orbitals are defined as the overlap between the wavefunction of an initial $N$-electron state ($|\Psi_0^N\rangle$) and the wavefunction of the final state with $N \pm 1$ electrons ($|\Psi_f^{N\pm1}\rangle$).

$$\phi_d(r_1) = \sqrt{N}\int \Psi^N(r_2,\ldots,r_N)\Psi^{N+1}(r_1,r_2,\ldots,r_N)\,dr_2\ldots dr_N \tag{2.15}$$

Because the the terms differ in one electron, the result of the overlap is a vector instead of a scalar, and can be expressed as a linear combination of the molecular orbitals ($\phi_p(r)$) of the reference wavefunction:

$$\phi_d(r) = \sum_p \gamma_p \phi_p(r) \tag{2.16}$$

where $\gamma_p$ are the coefficients that quantify the contribution of each molecular orbital to the Dyson orbital. Physically, Dyson orbitals can be interpreted as the correlated analog to the orbital of the electron that is either removed or attached.

The norm squared of the Dyson orbital, ($P$), is calculated by integrating the squared modulus of the Dyson orbital over all space:

$$P = \int |\phi_{Dyson}(r)|^2 \, dr = \sum_{p,q} \gamma_p^* \gamma_q \langle \phi_p | \phi_q \rangle \tag{2.17}$$

The pole strength ranges from 0 to 1 and provides a direct measure of the one-electron character of the ionization or electron attachment process. As the open shell wavefunction is usually obtained by means of a EOM-CC method, there are a 'left' and 'right' Dyson orbital.

They can be used for the interpretation and prediction of photoelectron spectra as they contain all the information required to calculate diffrential corss-sections, $\frac{d\sigma}{d\Omega_k}$:

$$\frac{d\sigma}{d\Omega_k} = \frac{4\pi^2 k E}{c} |\langle \phi_d | \mu | \Psi_k^{el} \rangle|^2 \tag{2.18}$$

where where $k$ is the magnitude of the photoelectron wavevector, $E$ is the energy of the ionizing radiation, and $c$ is the speed of light, $\mu$ is the dipole operator, and $\Psi_k^{el}$ is the photoelectron wavefunction, and a strong orthonormality is assumed between the reference and continuum wavefunction.

### 2.3.1 EOM-CC2 Dyson Orbital Equations

Justify that the expression doesnt change from CCSD (see TJ email).

#### EOM-EA-Dyson Equations

A derivation of the algebraic expression of Dyson orbitals in terms of the $t$, $r$, $l$, $\lambda$ amplitudes is presented. It is importnat to realize that the operators

involved ($\hat{T}, \hat{\Lambda}, \hat{R}, \hat{L}$) affect the occupation of the spin-orbitals, and thus only the combinations of terms which leave the refrence wavefunction, $|0\rangle$, unchanged survive. To find these combinations, commutators can be used to reorder the operators involved:

In the case of the right EOM-EA-Dyson orbital amplitudes:

$$\gamma_i^{\mathrm{EA,R}} = \langle EA|\hat{a}_i^\dagger|CC\rangle = \langle 0|\hat{L}^{EA}e^{-\hat{T}}\hat{a}_i^\dagger e^{\hat{T}}|0\rangle$$

The following equalities are usueful:

$$e^{-\hat{T}}e^{\hat{T}} = e^{\hat{T}}e^{-\hat{T}} = 1$$

$$[e^{\pm\hat{T}}, \hat{a}_p^\dagger] = \cancelto{0}{[1, \hat{p}^\dagger]} \pm t_j^b[\hat{b}^\dagger\hat{j}, \hat{p}^\dagger] \pm t_{jk}^{bc}[\hat{b}^\dagger\hat{c}^\dagger\hat{k}\hat{j}, \hat{p}^\dagger] + \dots$$

Where a change of notation, $a_p^\dagger \to p^\dagger$, upon expansion is done for readibility. Two cases are distinguished, $p$ is a virtual orbital, $a$, or an occupied orbital, $i$. For virtual orbitals, $p = a$:

$$[\hat{b}^\dagger\hat{j}, \hat{a}^\dagger] = \hat{b}^\dagger\hat{j}\hat{a}^\dagger - \hat{a}^\dagger\hat{b}^\dagger\hat{j} = (-1)^2\hat{a}^\dagger\hat{b}^\dagger\hat{j} - \hat{a}^\dagger\hat{b}^\dagger\hat{j} = 0$$

Similarly with higher order terms, it is arribed to:

$$[e^{\pm\hat{T}}, \hat{a}_a^\dagger] = 0$$

For occupied orbitals, $p = i$:

$$[\hat{b}^\dagger\hat{j}, \hat{\imath}^\dagger] = \hat{b}^\dagger\hat{j}\cancelto{0}{\hat{\imath}^\dagger} - \hat{\imath}^\dagger\hat{b}^\dagger\hat{j}$$

And similarly with higher order terms:

$$[e^{\pm\hat{T}}, \hat{a}_i^\dagger] = -\hat{a}_i^\dagger(e^{\pm\hat{T}} - 1)$$

These relations can now be used to derive the expression for the occupied and virtual Right EOM-EA-Dyson orbital amplitudes:

$$\phi_{\mathrm{D}}^{\mathrm{EA,R}} = \sum_p \gamma_p^{\mathrm{EA,R}}\phi_p = \sum_i^{\mathrm{occ}} \gamma_i^{\mathrm{EA,R}}\phi_i + \sum_a^{\mathrm{vir}} \gamma_a^{\mathrm{EA,R}}\phi_a$$

The general expression can be reordered:

$$\begin{aligned}\gamma_p^{\mathrm{EA,R}} &= \langle EA|\hat{a}_p^\dagger|CC\rangle = \langle 0|\hat{L}^{EA}e^{-\hat{T}}\hat{a}_p^\dagger e^{\hat{T}}|0\rangle \\ &= \langle 0|\hat{L}^{EA}(\hat{a}_p^\dagger e^{-\hat{T}} + [e^{-\hat{T}}, \hat{a}_p^\dagger])e^{\hat{T}}|0\rangle \end{aligned} \tag{2.19}$$

For virtual orbitals, $p = a$:

$$\begin{aligned}
\gamma_a^{\mathrm{EA,R}} &= \langle 0|\hat{L}^{EA}(\hat{a}_a^\dagger e^{-\hat{T}} + \cancelto{0}{[e^{-\hat{T}}, \hat{a}_a^\dagger]})e^{\hat{T}}|0\rangle \\
&= \langle 0|\hat{L}^{EA}\hat{a}_a^\dagger \cancelto{1}{e^{-\hat{T}}e^{\hat{T}}}|0\rangle = \langle 0|\hat{L}^{EA}\hat{a}_a^\dagger|0\rangle \\
&= \langle 0|l_a \hat{a}\hat{a}^\dagger|0\rangle \\
&= l_a
\end{aligned} \tag{2.20}$$

For occupied orbitals, $p = i$:

$$\begin{aligned}
\gamma_i^{\mathrm{EA,R}} &= \langle 0|\hat{L}^{EA}(\hat{a}_i^\dagger e^{-\hat{T}} + [e^{-\hat{T}}, \hat{a}_i^\dagger])e^{\hat{T}}|0\rangle \\
&= \langle 0|\hat{L}^{EA}(\cancelto{0}{\hat{a}_i^\dagger e^{-\hat{T}} - \hat{a}_i^\dagger e^{-\hat{T}}} + \hat{a}^\dagger)e^{\hat{T}}|0\rangle = \langle 0|\hat{L}^{EA}\hat{a}_i^\dagger e^{\hat{T}}|0\rangle \\
&= \langle 0|l_b t_i^b\, \hat{b}\hat{i}^\dagger\hat{b}^\dagger\hat{i} + l_{bc}^j t_{ij}^{bc}\, \hat{b}\hat{c}\hat{j}^\dagger\hat{i}^\dagger\hat{b}^\dagger\hat{c}^\dagger\hat{i}\hat{j}|0\rangle \\
&= -\sum_c t_{ic} l_c - \frac{1}{2}\sum_{kcd} t_{ki}^{dc} l_{dc}^k
\end{aligned} \tag{2.21}$$

A similar approach can be applyed to the other Dyson equations to obtain the expressions.

Left EOM-EA-Dyson orbital, $\phi_{\mathrm{D}}^{\mathrm{EA,L}} = \sum_i^{\mathrm{occ}} \gamma_i^{\mathrm{EA,L}}\phi_i + \sum_a^{\mathrm{vir}} \gamma_a^{\mathrm{EA,L}}\phi_a$:

$$\begin{aligned}
\gamma_i^{\mathrm{EA,L}} &= \langle CC|\hat{a}_i|EA\rangle \\
&= -\sum_c \lambda_{ic} r_c - \frac{1}{2}\sum_{kcd} \lambda_{ik}^{cd} r_k^{dc}
\end{aligned} \tag{2.22}$$

$$\begin{aligned}
\gamma_a^{\mathrm{EA,L}} &= \langle CC|\hat{a}_a|EA\rangle \\
&= r_a + \sum_{kc} \lambda_{kc} r_{ca}^k + \sum_k \gamma_k^{\mathrm{EA,L}} t_{ka} - \frac{1}{2}\sum_{klcd} \lambda_{lk}^{dc} t_{lk}^{da} r_c
\end{aligned} \tag{2.23}$$

### EOM-EA-EE-Dyson Equations

Right Dyson orbital, $\phi_{\mathrm{D}}^{\mathrm{EA-EE,R}} = \sum_i^{\mathrm{occ}} \gamma_i^{\mathrm{EA-EE,R}}\phi_i + \sum_a^{\mathrm{vir}} \gamma_a^{\mathrm{EA-EE,R}}\phi_a$:

$$\gamma_i^{\mathrm{EA-EE,R}} = \langle EA|\hat{a}_i^\dagger|EE\rangle$$
$$= r_0\gamma_a^{\mathrm{EA,R}} - \sum_c r_{ic}l_c - \frac{1}{2}\sum_{lcd} r_{il}^{cd}l_{dc}^{l} - \sum_{lcd} l_{dc}^{l}t_{ic}r_{ld} \tag{2.24}$$

$$\gamma_a^{\mathrm{EE-EA,R}} = \langle EA|\hat{a}_a^\dagger|EE\rangle$$
$$= r_0 l_a + \sum_{kc} l_{ca}^{k}r_{kc} \tag{2.25}$$

Left Dyson orbital, $\phi_{\mathrm{D}}^{\mathrm{EE-EA,L}} = \sum_i^{\mathrm{occ}} \gamma_i^{\mathrm{EE-EA,L}}\phi_i + \sum_a^{\mathrm{vir}} \gamma_a^{\mathrm{EE-EA,L}}\phi_a$:

$$\gamma_i^{\mathrm{EE-EA,L}} = \langle EE|\hat{a}_i|EA\rangle$$
$$= -\sum_c l_{ic}r_c - \frac{1}{2}\sum_{kcd} l_{ik}^{cd}r_k^{dc} \tag{2.26}$$

$$\gamma_a^{\mathrm{EE-EA,L}} = \langle EE|\hat{a}_a|EA\rangle$$
$$= \sum_{kc} l_{kc}r_{ca}^{k} + \sum_k \gamma_k^{\mathrm{EE-EA,L}}t_{ka} - \frac{1}{2}\sum_{klcd} l_{lk}^{dc}t_{lk}^{da}r_c \tag{2.27}$$

### EOM-IP-Dyson Equations

Right Dyson orbital, $\phi_{\mathrm{D}}^{\mathrm{EE,R}} = \sum_i^{\mathrm{occ}} \gamma_i^{\mathrm{IP,R}}\phi_i + \sum_a^{\mathrm{vir}} \gamma_a^{\mathrm{IP,R}}\phi_a$:

$$\gamma_a^{\mathrm{IP,R}} = \langle CC|\hat{a}_a^\dagger|IP\rangle$$
$$= \lambda_{ka}r_k + \frac{1}{2}\lambda_{lk}^{ca}r_{klc} \tag{2.28}$$

$$\gamma_i^{\mathrm{IP,R}} = \langle CC|\hat{a}_i^\dagger|IP\rangle$$
$$= r_i + \sum_{kc}\lambda_{kc}r_{ik}^{c} - \sum_c \gamma_c^{\mathrm{IP,R}}t_{ic} - \frac{1}{2}\sum_{klcd}\lambda_{lk}^{dc}t_{li}^{dc}r_k \tag{2.29}$$

Left Dyson orbital, $\phi_{\mathrm{D}}^{\mathrm{IP,L}} = \sum_i^{\mathrm{occ}} \gamma_i^{\mathrm{IP,L}} \phi_i + \sum_a^{\mathrm{vir}} \gamma_a^{\mathrm{IP,L}} \phi_a$:

$$\begin{aligned}\gamma_i^{\mathrm{IP,L}} &= \langle IP|\hat{a}_i|CC\rangle \\ &= l_i \end{aligned} \tag{2.30}$$

$$\begin{aligned}\gamma_a^{\mathrm{IP,L}} &= \langle IP|\hat{a}_a|CC\rangle \\ &= \sum_k t_{ka} l_k + \frac{1}{2}\sum_{klc} t_{kl}^{ac} l_{kl}^{c} \end{aligned} \tag{2.31}$$

### EOM-EE-IP-Dyson Equations

Right Dyson orbital, $\phi_{\mathrm{D}}^{\mathrm{EE-IP,R}} = \sum_i^{\mathrm{occ}} \gamma_i^{\mathrm{EE-IP,R}} \phi_i + \sum_a^{\mathrm{vir}} \gamma_a^{\mathrm{EE-IP,R}} \phi_a$:

$$\begin{aligned}\gamma_i^{\mathrm{EE-IP,R}} &= \langle EE|\hat{a}_i^\dagger|IP\rangle \\ &= \sum_{kc} l_{kc} r_{ik}^{c} - \sum_c \gamma_c^{IP-EI} t_{ic} - \frac{1}{2}\sum_{klcd} l_{lk}^{dc} t_{li}^{dc} r_k \end{aligned} \tag{2.32}$$

$$\begin{aligned}\gamma_a^{\mathrm{EE-IP,R}} &= \langle EE|\hat{a}_a^\dagger|IP\rangle \\ &= l_{ka} r_k + \frac{1}{2} l_{lk}^{ca} r_{klc} \end{aligned} \tag{2.33}$$

Left Dyson orbital, $\phi_{\mathrm{D}}^{\mathrm{IP-EE,L}} = \sum_i^{\mathrm{occ}} \gamma_i^{\mathrm{IP-EE,L}} \phi_i + \sum_a^{\mathrm{vir}} \gamma_a^{\mathrm{IP-EE,L}} \phi_a$:

$$\begin{aligned}\gamma_i^{\mathrm{IP-EE,L}} &= \langle IP|\hat{a}_i|EE\rangle \\ &= r_0 l_i + \sum_{kc} l_{ik}^{c} r_{kc} \end{aligned} \tag{2.34}$$

$$\begin{aligned}\gamma_a^{\mathrm{IP-EE,L}} &= \langle IP|\hat{a}_a|EE\rangle \\ &= r_0 \gamma_a^{\mathrm{IP,L}} + \sum_k r_{ka} l_k + \frac{1}{2}\sum_{klc} r_{kl}^{ac} l_{kl}^{c} + \sum_{klc} l_{kl}^{c} t_{ka} r_{cl} \end{aligned} \tag{2.35}$$

# Chapter 3

# Computational Methods

All electronic structure calculations were performed using the developer's copy of the *Q-Chem* software [31]. In all computations the frozen-core approximation is used, only the valence electrons are correlated, as well as the resolution of the identity (RI) approximation, auxiliary basis functions are used to approximate the two-electron integrals, reducing its scaling to $N(O^3)$ [32].

For the EOM-EA calculations, the reference wavefunction was obtained as the restricted Hartree-Fock (RHF) solution of the ground state of the neutral molecule. Unless explecitly mentioned, calculations were performed at using the aug-cc-pVDZ basis set [33] further augmented by 3 s-shells on hydrogen atoms and 6 s- and 3 p-shells on all non-hydrogen atoms [14] to properly model the non-valence states. The coefficients of the extra functions were obtained by successively halving the most diffuse function of the original set.

CC2 Dyson obitals for EOM variants described in section 2.3.1 and appendix **??** were implemented as described, and will be released in an upcoming verion of *Q-Chem*.

All closed-shell quinone model geometries were optimized using the TPSS functional[34] with Grimme's pair-wise dispersion corrections with Becke-Johnson damping (D3BJ)[35], and the minimally augmented[36] def2-TZVP basis sets[37] (ma-def2-TZVP), following the work in [38]. For the scan calculations, each singlepoint was optimized constraining its relevant angles by the method of Lagrange multipliers; dihedrals of the methoxy chains of Q0 and Q1,and the isoprene tail of Q1. In the case of quinone + aminoacid models, crystal structures were taken from the Protein Data Bank (PDB). Hydrogens were added using *PyMOL*'s [39] `add_H` functionality, and relaxed using the

method above (fixing the rest of the heavy atoms).

For the scans of quinone + molecule, each subsystem was independently optimized and and put together with any further refinement.

For quinone stystems, only EOM-EA right Dyson orbitals were computed to speed up the calculations by avoiding the need to compute the lamda terms.

Photoionization and Photodetachment crossections were calculated using the *ezDyson* package [40, 41].

# Chapter 4

# Results and Discussion

## 4.1 Performance of EOM-CC2 Related Methods

...

### 4.1.1 Basis Set Dependence of EA-EOM-CC2 in Dipole Bound Anions

...

| | | RI-CC2 | | | | | | RI-CCSD | | | |
|---|---|---|---|---|---|---|---|---|---|---|---|
| | | | aug-cc-pVTZ | | | pVDZ | pVQZ | pVDZ | pTDZ | | |
| Molecule | | 2s1p | 4s2p | 6s3p | 8s4p | 6s3p | 6s3p | 6s3p | 6s3p | KT | μ(D) |
| Acetaldehyde | $CH_3CHO$ | -156.7 | -27.8 | -3.2 | 0.8 | -4.6 | -3.2 | -4.6 | -3.1 | -0.4 | 3.29 |
| Acetone | $(CH_3)_2CO$ | -114.9 | -16.8 | 1.3 | 3.3 | -0.3 | 0.9 | -0.5 | 0.9 | -5.1 | 3.46 |
| Acetonitrile | $CH_3CN$ | -61.2 | 12.6 | 19.9 | 20.1 | 18.2 | 20.3 | 17.1 | 18.4 | 4.2 | 4.29 |
| Benzaldehyde | $C_6H_5CHO$ | -97.1 | -2.1 | 8.9 | 9.6 | 7.4 | 9.1 | 3.4 | 4.6 | -4.9 | 3.77 |
| N,N-Dimethylformamide | $(CH_3)_2NCHO$ | -81.1 | 5.4 | 14.1 | 14.4 | 13.2 | 14.4 | 13.3 | 13.7 | 1.9 | 4.48 |
| DMSO | $(CH_3)_2SO$ | -84.5 | 4.0 | 15.4 | 16.1 | 14.8 | 15.5 | 14.7 | 14.9 | 2.1 | 4.63 |
| Formamide | $CH_3NO$ | -92.2 | 1.1 | 16.2 | 17.2 | 15.1 | 17.0 | 15.1 | 15.9 | 3.4 | 4.28 |
| Methylisocyanide | $CH_3NC$ | -95.1 | -0.5 | 10.0 | 10.5 | 9.5 | 10.1 | 8.8 | 9.0 | -1.8 | 3.59 |
| Nitrobenzene | $C_6H_5NO_2$ | -63.6 | 30.6 | 34.8 | 34.8 | 32.5 | - | 25.0 | 25.9 | 5.4 | 5.15 |
| Nitromethane | $CH_3NO_2$ | -82.9 | 5.7 | 14.2 | 14.7 | 13.0 | 14.7 | 12.9 | 13.7 | 3.5 | 4.10 |
| Nitrosobenzene | $C_6H_5NO$ | -125.0 | 1.0 | 11.4 | - | 9.9 | - | 5.1 | 6.0 | -4.1 | 3.73 |
| Phenylisocyanide | $C_6H_5NC$ | -82.7 | 8.6 | 16.3 | 16.5 | 15.2 | 16.7 | 9.0 | 9.2 | -4.9 | 3.61 |
| Pyridazine | $C_4H_4N_2$ | -80.7 | 20.5 | 26.3 | 26.4 | 25.0 | 26.7 | 18.6 | 19.1 | 1.7 | 4.41 |
| Vinylene carbonate | $C_3H_2O_3$ | -82.5 | 20.9 | 27.2 | 27.4 | 26.4 | 27.7 | 25.1 | 25.5 | 10 | 5.05 |
| | MAE | 105.3 | 8.8 | 2.8 | 3.4 | 2.3 | 2.4 | 0.8 | ref. | 12.0 | |

Table 4.1: EOM-EA binding energies of dipole-bound radical anions computed using different augmented Dunning basis sets and RI-CC2 and RI-CCSD for the the test set of moluces [14]. A positive value corresponds to a bound electron. Koopmans' theorem (KT), and dipole momment (μ), calculated at the HF level, and mean absolute error (MAE) are also given. The values are in meV and D respectively.

### 4.1.2 Performance of EA-EOM-CC2 on Valence Bound Radical Anion States of Quinones

| Mol. | Ref. [38] | | RI-CC2 | |
|---|---|---|---|---|
| | Exp (aEA) | CCSD(T) $+E_{CBS}$ | No SCS | SCS |
| 1 | 1.91 | 1.64 | 2.02 | 1.54 |
| 2 | 1.85 | 1.57 | 1.95 | - |
| 3 | 1.76 | 1.49 | 1.89 | 1.39 |
| 4 | 1.77 | 1.5 | 1.89 | 1.40 |
| 5 | 1.69 | 1.43 | 1.84 | 1.34 |
| 6 | 1.62 | 1.42 | 1.83 | 1.32 |
| 7 | 1.72 | 1.32 | 1.65 | 1.17 |
| 8 | 1.86 | 1.5 | 1.88 | 1.39 |
| 9 | 1.81 | 1.55 | 1.97 | - |
| 10 | 1.74 | 1.51 | 1.92 | 1.45 |

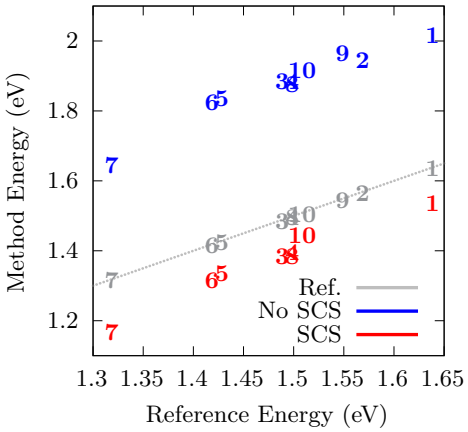


**Table 4.2** and **Figure 4.1:** Comparison between reference and RI-CC2 data for quinones. The table also includes the experimental value (adiabatic EA instead of veritacl EA).

SCS improves the result for valence state of CC2, whihc is in accordance with the conclusions from [14]. Something to note is that when comparing the results with experiments, one can think that CC2 gets close than CCSD. This however, can be explained by the fact that the experiment measures the adiabatic electron binding energy, while the calculations are performed for the vertical EA. As the former energy

As the trend is recovered without SCS, albeit the larger ( 0.2 eV) but consist error the subsequent calculations do not use this method, as SCS worsens the results for dipole bound anions. A strength of this approach is that both states can be calculated from the same Hamiltonian, and the results are consitent.

Dipole bound states are worsen by SCS [14]. This is explaned by the fact that the DBS resides in a digguse state; the extra spin is far from the other electrons, meaning that the exchange interaction is much smaller than the Coulumb interaction. ...

### 4.1.3 Photoelectron Cross-section Calculations from EOM-CC2/CCSD

...

## 4.2 Study on the Anion States of Ubiquinone

...

### 4.2.1 Energy and Dipole Surfaces of CoQ

...

#### Q0

aa

...

#### Q1

...

### 4.2.2 A Simple Cluster Model

...

### 4.2.3 Interaction with Water

...

### 4.2.4 Effect of Nearby Amionacids

...

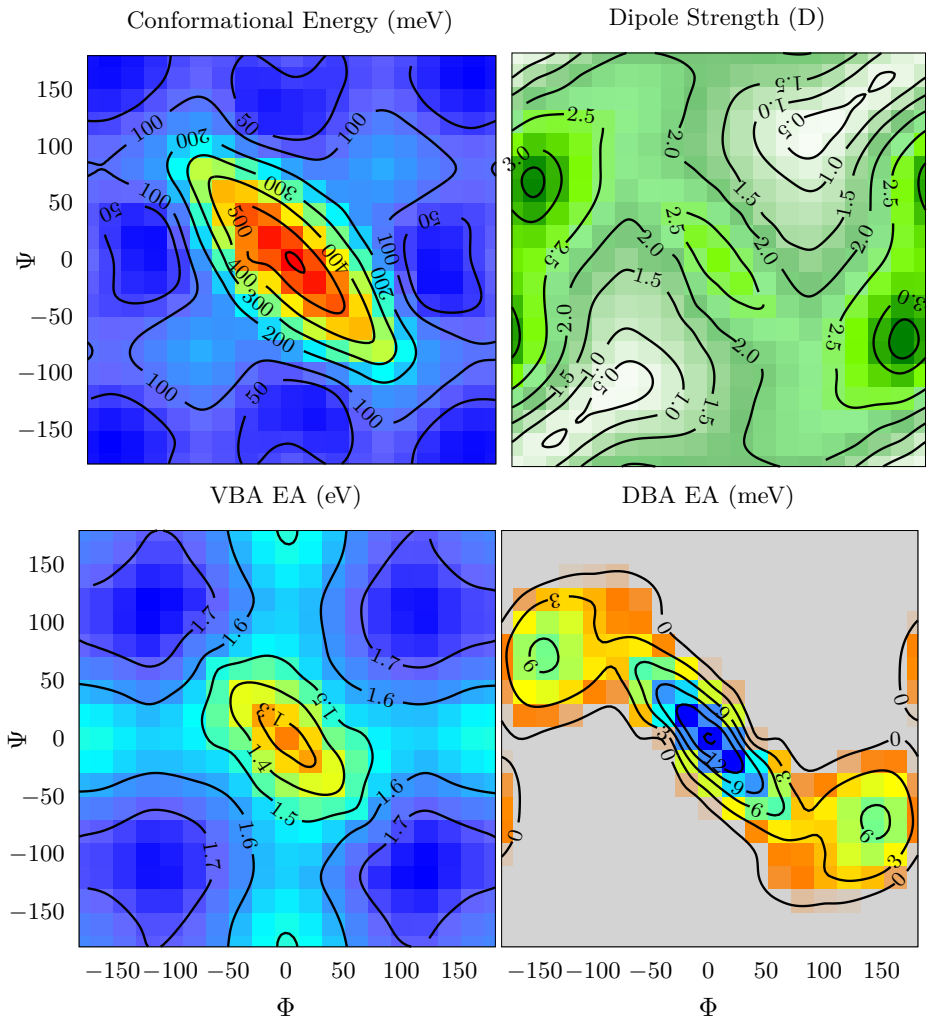


Figure 4.2: Surfaces of Q0. Left: Energy surface. Right: Dipole moment surface.

### Serine

...

### Threonine

...

### Apsaragine

...

### Isoleucine

...

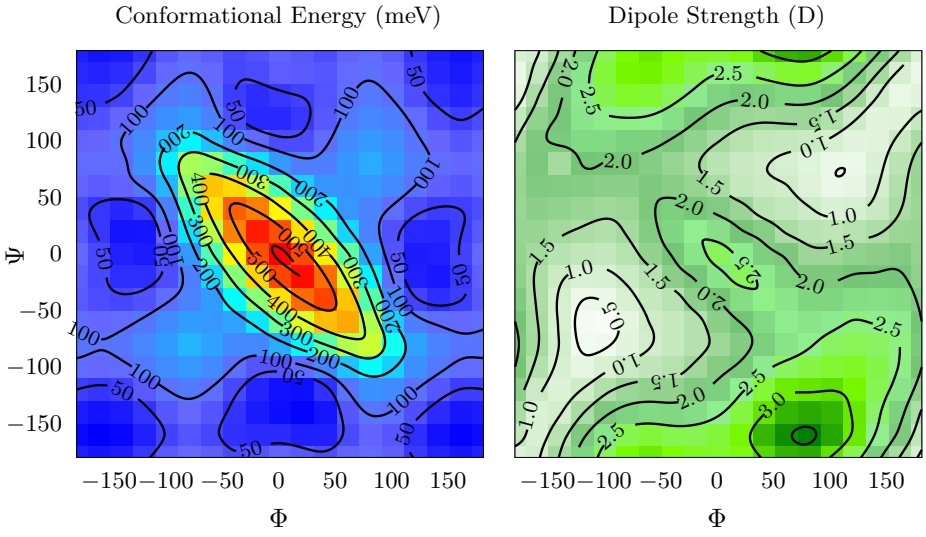


Figure 4.3: Surfaces of Q1. Left: Energy surface. Right: Dipole moment surface.

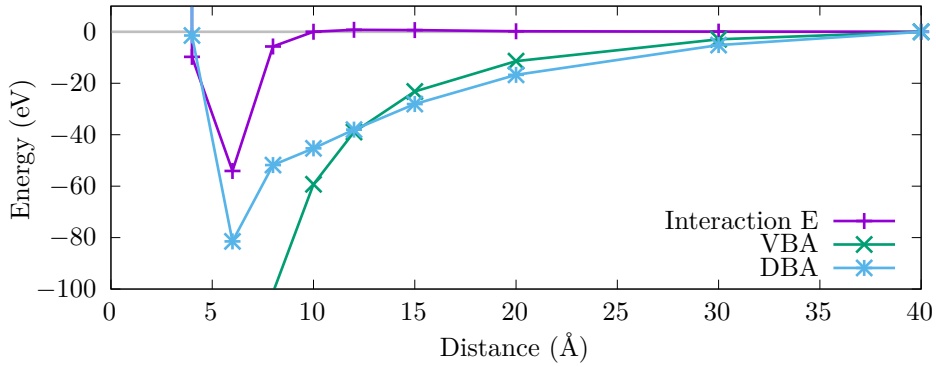


Figure 4.4: Favorable Interaction with water.

# Chapter 5

# This is conclusion

...

**Instructions by the Arenberg Doctoral School:**

An extensive conclusion, including a global discussion of the research results, a discussion of the implications of the PhD research and future perspectives in regards to follow-up research.

# Appendix A

# This is myappendix

...

**Instructions by the Arenberg Doctoral School:**

Appendices: The appendices should include parts of the research which are essential for the work, but which may hamper the readability of the text, e.g. because of their length (mathematical deductions, experimental data, examples, figures, etc.).

# Bibliography

[1] Jack Simons. Molecular anions. *The Journal of Physical Chemistry A*, 112(29):6401–6511, 2008.

[2] John M Herbert. The quantum chemistry of loosely-bound electrons. *Reviews in Computational Chemistry Volume 28*, pages 391–517, 2015.

[3] H Abdoul-Carime and C Desfrançois. Electrons weakly bound to molecules by dipolar, quadrupolar or polarization forces. *The European Physical Journal D-Atomic, Molecular, Optical and Plasma Physics*, 2:149–156, 1998.

[4] Jack Simons. Molecular anions perspective. *The Journal of Physical Chemistry A*, 127(18):3940–3957, 2023.

[5] Kenneth D Jordan and Feng Wang. Theory of dipole-bound anions. *Annual review of physical chemistry*, 54(1):367–396, 2003.

[6] Enrico Fermi and Edward Teller. The capture of negative mesotrons in matter. *Physical Review*, 72(5):399, 1947.

[7] Do Hyung Kang and Sang Kyu Kim. Reaction dynamics of the nonvalence bound states of the anions. *Chemical Physics Reviews*, 5(4), 2024.

[8] Ryan C Fortenberry. Interstellar anions: the role of quantum chemistry. *The Journal of Physical Chemistry A*, 119(39):9941–9953, 2015.

[9] Jishnu Narayanan SJ, Divya Tripathi, Pooja Verma, Amitava Adhikary, and Achintya Kumar Dutta. Secondary electron attachment-induced radiation damage to genetic materials. *ACS omega*, 8(12):10669–10689, 2023.

[10] Barbora Sedmidubská and Jaroslav Kočišek. Interaction of low-energy electrons with radiosensitizers. *Physical Chemistry Chemical Physics*, 26(12):9112–9136, 2024.

[11] Stephen E Bradforth and Pavel Jungwirth. Excited states of iodide anions in water: A comparison of the electronic structure in clusters and in bulk solution. *The Journal of Physical Chemistry A*, 106(7):1286–1298, 2002.

[12] Hsing-Yin Chen and Wen-Shyan Sheu. Precursors of the charge-transfer-to-solvent states in i-(h2o) n clusters. *Journal of the American Chemical Society*, 122(31):7534–7542, 2000.

[13] John M Herbert and Marc P Coons. The hydrated electron. *Annual review of physical chemistry*, 68(1):447–472, 2017.

[14] Garrette Pauley Paran, Cansu Utku, and Thomas-Christian Jagau. On the performance of second-order approximate coupled-cluster singles and doubles methods for non-valence anions. *Physical Chemistry Chemical Physics*, 26(3):1809–1818, 2024.

[15] Piotr Skurski, Maciej Gutowski, and Jack Simons. How to choose a one-electron basis set to reliably describe a dipole-bound anion. *International Journal of Quantum Chemistry*, 80(4-5):1024–1038, 2000.

[16] Maciej Gutowski, Piotr Skurski, Alexander I Boldyrev, Jack Simons, and Kenneth D Jordan. Contribution of electron correlation to the stability of dipole-bound anionic states. *Physical Review A*, 54(3):1906, 1996.

[17] Guillaume Thiam and Franck Rabilloud. How accurately can dft describe non-valence anions? *Journal of Chemical Theory and Computation*, 19(10):2842–2849, 2023.

[18] Iwona Anusiewicz, Piotr Skurski, and Jack Simons. Fate of dipole-bound anion states when hydrated. *The Journal of Physical Chemistry A*, 124(10):2064–2076, 2020.

[19] Maria Elena Castellani, Cate S Anstöter, and Jan RR Verlet. On the stability of a dipole-bound state in the presence of a molecule. *Physical Chemistry Chemical Physics*, 21(44):24286–24290, 2019.

[20] Jishnu Narayanan SJ, Pooja Verma, Amitava Adhikary, and Achintya Kumar Dutta. Electron attachment to the nucleobase uracil in diethylene glycol: The signature of a doorway. *ChemPhysChem*, 25(24):e202400581, 2024.

[21] Jiande Gu, Jerzy Leszczynski, and Henry F Schaefer III. Interactions of electrons with bare and hydrated biomolecules: From nucleic acid bases to dna segments. *Chemical reviews*, 112(11):5603–5640, 2012.

[22] Edward Matthews and Caroline EH Dessent. Observation of near-threshold resonances in the flavin chromophore anions alloxazine and lumichrome. *The Journal of Physical Chemistry Letters*, 9(20):6124–6130, 2018.

[23] Jiakuan Chen, Andrzej Pelc, João Ameixa, Fábris Kossoski, and Stephan Denifl. Low-energy electron interactions with methyl-p-benzoquinone: A study of negative ion formation. *ACS omega*, 9(36):38032–38043, 2024.

[24] William James Russell. Address to the chemical section. *Chemical News and Journal of Physical Science*, 28:148–153, 1873.

[25] Lars Ernster and Gustav Dallner. Biochemical, physiological and medical aspects of ubiquinone function. *Biochimica et Biophysica Acta (BBA)-Molecular Basis of Disease*, 1271(1):195–204, 1995.

[26] J Ameixa, E Arthur-Baidoo, J Pereira-da Silva, M Ončák, JC Ruivo, MT do N Varella, F Ferreira Da Silva, and S Denifl. Parent anion radical formation in coenzyme q0: Breaking ubiquinone family rules. *Computational and Structural Biotechnology Journal*, 21:346–353, 2023.

[27] Christopher W West, James N Bull, Erkki Antonkov, and Jan RR Verlet. Anion resonances of para-benzoquinone probed by frequency-resolved photoelectron imaging. *The Journal of Physical Chemistry A*, 118(48):11346–11354, 2014.

[28] Stanislav A Pshenichnyuk, Alberto Modelli, Nail L Asfandiarov, and Alexey S Komolov. Ionizing radiation and natural constituents of living cells: low-energy electron interaction with coenzyme q analogs. *The Journal of chemical physics*, 153(11), 2020.

[29] James N Bull, Christopher W West, and Jan RR Verlet. Anion resonances and above-threshold dynamics of coenzyme q 0. *Physical Chemistry Chemical Physics*, 17(24):16125–16135, 2015.

[30] Attila Szabo and Neil S Ostlund. *Modern quantum chemistry: introduction to advanced electronic structure theory*. Courier Corporation, 1996.

[31] Evgeny Epifanovsky, Andrew T. B. Gilbert, Xintian Feng, Joonho Lee, Yuezhi Mao, Narbe Mardirossian, Pavel Pokhilko, Alec F. White, Marc P. Coons, Adrian L. Dempwolff, Zhengting Gan, Diptarka Hait, Paul R. Horn, Leif D. Jacobson, Ilya Kaliman, Jörg Kussmann, Adrian W. Lange, Ka Un Lao, Daniel S. Levine, Jie Liu, Simon C. McKenzie, Adrian F. Morrison, Kaushik D. Nanda, Felix Plasser, Dirk R. Rehn, Marta L. Vidal, Zhi-Qiang You, Ying Zhu, Bushra Alam, Benjamin J. Albrecht, Abdulrahman Aldossary, Ethan Alguire, Josefine H. Andersen, Vishikh Athavale, Dennis Barton, Khadiza Begam, Andrew Behn, Nicole Bellonzi, Yves A. Bernard,

Eric J. Berquist, Hugh G. A. Burton, Abel Carreras, Kevin Carter-Fenk, Romit Chakraborty, Alan D. Chien, Kristina D. Closser, Vale Cofer-Shabica, Saswata Dasgupta, Marc de Wergifosse, Jia Deng, Michael Diedenhofen, Hainam Do, Sebastian Ehlert, Po-Tung Fang, Shervin Fatehi, Qingguo Feng, Triet Friedhoff, James Gayvert, Qinghui Ge, Gergely Gidofalvi, Matthew Goldey, Joe Gomes, Cristina E. González-Espinoza, Sahil Gulania, Anastasia O. Gunina, Magnus W. D. Hanson-Heine, Phillip H. P. Harbach, Andreas Hauser, Michael F. Herbst, Mario Hernández Vera, Manuel Hodecker, Zachary C. Holden, Shannon Houck, Xunkun Huang, Kerwin Hui, Bang C. Huynh, Maxim Ivanov, Ádám Jász, Hyunjun Ji, Hanjie Jiang, Benjamin Kaduk, Sven Kähler, Kirill Khistyaev, Jaehoon Kim, Gergely Kis, Phil Klunzinger, Zsuzsanna Koczor-Benda, Joong Hoon Koh, Dimitri Kosenkov, Laura Koulias, Tim Kowalczyk, Caroline M. Krauter, Karl Kue, Alexander Kunitsa, Thomas Kus, István Ladjánszki, Arie Landau, Keith V. Lawler, Daniel Lefrancois, Susi Lehtola, Run R. Li, Yi-Pei Li, Jiashu Liang, Marcus Liebenthal, Hung-Hsuan Lin, You-Sheng Lin, Fenglai Liu, Kuan-Yu Liu, Matthias Loipersberger, Arne Luenser, Aaditya Manjanath, Prashant Manohar, Erum Mansoor, Sam F. Manzer, Shan-Ping Mao, Aleksandr V. Marenich, Thomas Markovich, Stephen Mason, Simon A. Maurer, Peter F. McLaughlin, Maximilian F. S. J. Menger, Jan-Michael Mewes, Stefanie A. Mewes, Pierpaolo Morgante, J. Wayne Mullinax, Katherine J. Oosterbaan, Garrette Paran, Alexander C. Paul, Suranjan K. Paul, Fabijan Pavošević, Zheng Pei, Stefan Prager, Emil I. Proynov, Ádám Rák, Eloy Ramos-Cordoba, Bhaskar Rana, Alan E. Rask, Adam Rettig, Ryan M. Richard, Fazle Rob, Elliot Rossomme, Tarek Scheele, Maximilian Scheurer, Matthias Schneider, Nickolai Sergueev, Shaama M. Sharada, Wojciech Skomorowski, David W. Small, Christopher J. Stein, Yu-Chuan Su, Eric J. Sundstrom, Zhen Tao, Jonathan Thirman, Gábor J. Tornai, Takashi Tsuchimochi, Norm M. Tubman, Srimukh Prasad Veccham, Oleg Vydrov, Jan Wenzel, Jon Witte, Atsushi Yamada, Kun Yao, Sina Yeganeh, Shane R. Yost, Alexander Zech, Igor Ying Zhang, Xing Zhang, Yu Zhang, Dmitry Zuev, Alán Aspuru-Guzik, Alexis T. Bell, Nicholas A. Besley, Ksenia B. Bravaya, Bernard R. Brooks, David Casanova, Jeng-Da Chai, Sonia Coriani, Christopher J. Cramer, György Cserey, A. Eugene DePrince, Robert A. DiStasio, Andreas Dreuw, Barry D. Dunietz, Thomas R. Furlani, William A. Goddard, Sharon Hammes-Schiffer, Teresa Head-Gordon, Warren J. Hehre, Chao-Ping Hsu, Thomas-C. Jagau, Yousung Jung, Andreas Klamt, Jing Kong, Daniel S. Lambrecht, WanZhen Liang, Nicholas J. Mayhall, C. William McCurdy, Jeffrey B. Neaton, Christian Ochsenfeld, John A. Parkhill, Roberto Peverati, Vitaly A. Rassolov, Yihan Shao, Lyudmila V. Slipchenko, Tim Stauch, Ryan P. Steele, Joseph E. Subotnik, Alex J. W. Thom, Alexandre Tkatchenko, Donald G. Truhlar, Troy Van Voorhis, Tomasz A.

Wesolowski, K. Birgitta Whaley, H. Lee Woodcock, Paul M. Zimmerman, Shirin Faraji, Peter M. W. Gill, Martin Head-Gordon, John M. Herbert, and Anna I. Krylov. Software for the frontiers of quantum chemistry: An overview of developments in the q-chem 5 package. *J. Chem. Phys.*, 155(8):084801, 2021.

[32] Christof Hättig and Florian Weigend. Cc2 excitation energy calculations on large molecules using the resolution of the identity approximation. *The Journal of Chemical Physics*, 113(13):5154–5161, 2000.

[33] Thom H Dunning Jr. Gaussian basis sets for use in correlated molecular calculations. i. the atoms boron through neon and hydrogen. *The Journal of chemical physics*, 90(2):1007–1023, 1989.

[34] Jianmin Tao, John P Perdew, Viktor N Staroverov, and Gustavo E Scuseria. Climbing the density functional ladder: Nonempirical meta–generalized gradient approximation designed for molecules and solids. *Physical review letters*, 91(14):146401, 2003.

[35] Stefan Grimme, Stephan Ehrlich, and Lars Goerigk. Effect of the damping function in dispersion corrected density functional theory. *Journal of computational chemistry*, 32(7):1456–1465, 2011.

[36] Jingjing Zheng, Xuefei Xu, and Donald G Truhlar. Minimally augmented karlsruhe basis sets. *Theoretical Chemistry Accounts*, 128:295–305, 2011.

[37] Florian Weigend and Reinhart Ahlrichs. Balanced basis sets of split valence, triple zeta valence and quadruple zeta valence quality for h to rn: Design and assessment of accuracy. *Physical Chemistry Chemical Physics*, 7(18):3297–3305, 2005.

[38] Christine E Schulz, Achintya Kumar Dutta, Róbert Izsák, and Dimitrios A Pantazis. Systematic high-accuracy prediction of electron affinities for biological quinones. *Journal of Computational Chemistry*, 39(29):2439–2451, 2018.

[39] Schrödinger, LLC. The PyMOL molecular graphics system. 2015.

[40] Samer Gozem and Anna I Krylov. The ezspectra suite: An easy-to-use toolkit for spectroscopy modeling. *Wiley Interdisciplinary Reviews: Computational Molecular Science*, 12(2):e1546, 2022.

[41] Samer Gozem and Anna I Krylov. Photoionization and photodetachment spectra from equation-of-motion coupled-cluster dyson orbitals. *Chem. Lett*, 6:4532–4540, 2015.

# Statement on the use of Generative AI

**Instructions by the Arenberg Doctoral School:**

Read the guidelines in relation to GenAI at KU Leuven and add the 'statement on the use of Generative AI' in your manuscript.

Generative AI was used for lenguage and coding assistance (ChatGPT, MicrosoftCopilot, LeChat).
The text, code, and images in this thesis are my own (unless otherwise specified). Generative AI has only been used in accordance with the KU Leuven guidelines and appropriate references have been added. I have reviewed and edited the content as needed and I take full responsibility for the content of the thesis.

DEPARTMENT OF CHEMISTRY
DEPARTMENT OF CHEMISTRY
Celestijnenlaan 200A box 2402
B-3001 Leuven
first.name@dept.kuleuven.be
https://chem.kuleuven.be/en/research/qcpc/tue/